High-intensity localized structures in the degenerate optical parametric oscillator: Comparison between the propagation and the mean-field models

M. Tlidi
Optique Nonlinéaire Théorique, Université Libre de Bruxelles, Campus Plaine, CP 231, B-1050 Bruxelles, Belgium

M. Le Berre, E. Ressayre, and A. Tallet
Laboratoire de Photophysique Moléculaire, Bâtiment 210, Université Paris–Sud, 91405 Orsay Cedex, France

L. Di Menza
Laboratoire d'Analyse Numerique et EDP, Bâtiment 425, Université Paris–Sud, 91405 Orsay Cedex, France
(Received 24 March 1999; published 13 March 2000)

The degenerate optical parametric oscillator may generate very high-intensity two-dimensional localized structures. A quantitative comparison of the propagation and the mean-field models is presented for different mistunings, corresponding to monostable and bistable homogeneous solutions. In both models, we study the circular domain walls as an example of localized structures. The peak intensities are comparable; the difference lies mainly in their domain of existence as a function of the pump amplitude parameter.

PACS number(s): 42.65.Sf, 42.60.Mi

I. INTRODUCTION

The electromagnetic field-matter interaction is generally described by a reduced Maxwell equation with a source obeying the Bloch equation in the case of an atomic or molecular system. In the case where the source behaves like a Kerr medium in a cavity operating on a single longitudinal mode, Lugiato and Lefever [1] developed the so-called mean-field (or uniform-field) model that reduces the original equations to a single partial differential equation for the electric field. The method relies on a perturbation expansion assuming a small transmittivity, a small field amplitude compared to the saturation amplitude, and a response time in between the delay and the cavity photon lifetime. The predictions of the mean-field model were found to agree fairly well with the experimental observations in the case of a confocal cavity with curvature mirrors [2].

Later on, the mean-field model was extended to other nonlinear media, such as $\chi^{(2)}$ crystals [3,4]. In this case, the mean-field model leads to two coupled partial differential equations, in the case of either second harmonic generation or a degenerate optical parametric oscillator (DOPO).

Within the mean-field model, it is easy to derive envelope equations, such as the Swift-Hohenberg, Ginzburg-Landau, or nonlinear Schrödinger equations. A description in terms of these amplitude equations is especially useful for the DOPO. Two approaches were proposed, in two different limits. The first consists of an adiabatic elimination of the pump field leading to a nonlinear Schrödinger equation with damping and parametric gain [5]. The second describes the vicinity of the lasing threshold where the transverse effects apprear via a diffusive equation of the Swift-Hohenberg type [6]. Both models predicted the occurrence of domain walls.

The relevance of these predictions for the DOPO has not yet been proved, but fronts and circular domain walls were recently observed in a photorefractive oscillator [7]. The experimental profiles and those derived from the Swift-Hohenberg equation [6] have much in common, but undoubtedly are only qualitatively similar.

The purpose of this paper is to compare quantitatively numerical simulations of the reduced Maxwell equations plus the boundary conditions, or propagation model [8], and those of the mean-field model for the DOPO. Both models display domain walls [9].

The system operates on a single longitudinal mode, and the transmittivity factor is small, varying between 10^{-1} and 10^{-2}, in order to fulfill the basic requirements for the validity of the mean-field model. Other parameters have been chosen such that domain walls occur and the comparison between both models has focused on the circular domain walls, where large intensity peaks can be generated. Several questions arise: Does the mean-field model reproduce propagation model results in the limit where signal and pump amplitudes reach values close to unity? Is the agreement between the propagation model and the mean-field model improved as the transmittivity factor vanishes?

In Sec. II, the mean-field model is derived from the propagation model, and the scalings for the reduced mean-field quantities are given. This derivation is presented to display the successive approximations necessary to achieve the mean-field equations for the DOPO. This makes a comparison between the two theories easier. In Sec. III, a linear stability analysis (LSA) of the homogeneous nontrivial solutions for the pump and signal fields is derived within the mean-field limit. The LSA for the propagation model cannot be completed analytically; nevertheless under some limited expansion for the solutions of pump and signal amplitudes, it was already presented and discussed with respect to the numerical results [9]. Finally in Sec. IV, a numerical comparison is shown for two sets of mistunings for which circular domain walls with large maxima occur. We conclude in Sec. V.

II. PROPAGATION AND MEAN-FIELD MODELS

We consider a planar cavity, driven by a coherent plane-wave field at a frequency ω_0, filled with the $\chi^{(2)}$ nonlinear medium in which parametric down-conversion takes place: one photon with frequency ω_0 is absorbed and two photons with frequencies $\omega_0/2$ are emitted. The optical cavity can be either a ring cavity of length l or a Fabry-Pérot cavity of length $l/2$. Such a configuration settles a single longitudinal mode.

The pump and signal amplitudes $\alpha_0(z,\tau,x,y)$ and $\alpha_1(z,\tau,x,y)$, respectively, associated with driving frequencies ω_0 and $\omega_1=\omega_0/2$, satisfy the following reduced Maxwell equations when propagating inside the $\chi^{(2)}$ crystal of length l:

$$\partial_z\alpha_0=\frac{i}{2}\nabla^2\alpha_0+i\alpha_1^2e^{i\Delta kz}, \tag{1}$$

$$\partial_z\alpha_1=i\nabla^2\alpha_1+i\alpha_0\alpha_1^*e^{-i\Delta kz}. \tag{2}$$

The transverse Laplacian $\nabla^2=(\partial_x^2+\partial_y^2)/_2k_1$ describes the diffraction effect on the transverse plane (x,y) with $k_1=\omega_1/c$, z is the longitudinal coordinate along the propagation axis, τ is the retarded time, and c is the velocity of light. The phase mismatch between the pump and the signal is $\Delta k=2n_1k_1-n_0k_0$, where the mistunings $\theta_{1,0}$ are defined by $\theta_{1,0}=n_{1,0}k_{1,0}l-2\pi$ and $n_{1,0}$ are the linear refractive indexes corresponding, respectively, to the pump and signal fields. In order to satisfy the phase-matching condition, the ratio between the diffraction of the two fields is fixed [10].

The propagation equations (1) and (2) must be completed with the boundary conditions

$$\alpha_0(0,x,y,\tau)=\alpha_0^{in}+R_0e^{i\theta_0}\alpha_0(l,x,y,\tau-d), \tag{3}$$

$$\alpha_1(0,x,y,\tau)=R_1e^{i\theta_1}\alpha_1(l,x,y,\tau-d) \tag{4}$$

where d is the delay time l/c and $R_{0,1}$ denote the reflectivity factors for pump and signal fields, respectively. α_0^{in} is the amplitude of the driven field. These two sets of equations (1)–(4) provide what we call the propagation model, in opposition to the mean-field model [11]. The latter can be easily derived from the above equations: First, the solutions for the pump and signal amplitudes at the crystal exit are approximated from the reduced Maxwell equations as the first-order terms of the Mac-Laurin expansion, i.e.,

$$\alpha_0(1,x,y,\tau)=\alpha_0(0,x,y,\tau)+\frac{i}{2}\nabla^2\alpha_0(0,x,y,\tau)+i\alpha_1^2(0,x,y,\tau), \tag{5}$$

$$\alpha_1(1,x,y,\tau)=\alpha_1(0,x,y,\tau)+i\nabla^2\alpha_1(0,x,y,\tau)+i\alpha_0(0,x,y,\tau)\alpha_1^*(0,x,y,\tau), \tag{6}$$

with the rescaling $\alpha_{i,j}\rightarrow l\alpha_{i,j}$. These solutions are valid in the limit of small amplitudes

$$|\alpha_{0,1}|\ll 1, \tag{7}$$

and for negligible terms resulting of any operator ∇^{2n} with $n>2$.

The approximate solutions (5) and (6) are introduced in the right-hand members of Eqs. (3) and (4). Then, assuming that the time variation of these solutions is very slow as compared to the delay d, i.e.,

$$\alpha_{0,1}(0,x,y,\tau+d)=\alpha_{0,1}(0,x,y,\tau)+d\partial_\tau\alpha_{0,1}(0,x,y,\tau), \tag{8}$$

unscaled forms of the mean-field equations are

$$d\partial_\tau\alpha_0=\alpha_0^{in}-(1-R_0e^{i\theta_0})\alpha_0+\frac{iR_0e^{i\theta_0}}{2}[\nabla^2\alpha_0+2\alpha_1^2], \tag{9}$$

$$d\partial_\tau\alpha_1=-(1-R_1e^{i\theta_1})\alpha_1+iR_1e^{i\theta_1}[\nabla^2\alpha_1+\alpha_1^*\alpha_0], \tag{10}$$

with $\alpha_{0,1}=\alpha_{0,1}(0,x,y,\tau)$. Two further assumptions consist of large reflectivity $R_{0,1}\simeq 1$ and small detunings $\theta_{0,1}\ll 1$, or $e^{i\theta_{0,1}}\rightarrow(1+i\theta_{0,1})$. Then, rescaling the time and space variables and using the rescaled quantities [9],

$$(A_0,A_1,E,\Delta_{0,1})=\left(\frac{i\alpha_0}{1-R_1},\frac{\alpha_1}{1-R_1},\frac{i\alpha_0^{in}}{(1-R_1)^2},\frac{-\theta_{0,1}}{1-R_1}\right), \tag{11}$$

$$[\tau(1-R_1)/d,\nabla^2]\rightarrow[\tau,\nabla^2/(1-R_1)] \tag{12}$$

gives rise to the mean-field equations for the DOPO,

$$\partial_\tau A_0=E-(\gamma+i\Delta_0)A_0+\frac{i}{2}\nabla^2A_0-A_1^2, \tag{13}$$

$$\partial_\tau A_1=-(1+i\Delta_1)A_1+i\nabla^2A_1+A_0A_1^*, \tag{14}$$

with $\gamma=(1-R_0)/(1-R_1)$.

The scaled and unscaled partial differential equations (9) and (10) and (13) and (14), respectively, look the same, except that the reflectivity factors do not explicitly appear in the mean-field equations in the case $R_0=R_1$. The mean-field amplitudes $A_{0,1}$ can be arbitrarily large while the unscaled ones have to be smaller than unity; the same remark holds for the scaled mistunings. For instance, Eqs. (13) and (14) were shown to reduce to a single nonlinear Schrödinger equation with damping and parametric gain [5] in the limits $\Delta_0\gg 1$ and $\Delta_0/\Delta_1\gg 1$. This derivation was performed without specifying the actual values of R_1, θ_0, and θ_1, while small values of θ_0 and θ_1 are required in order to derive Eqs. (13) and (14) from the unscaled equations (9) and (10).

The propagation equations depend explicitly on the reflectivity factors. These factors have to be varied when comparing the numerical simulations of the propagation model with those for the mean-field model, in order to learn in which domain of the reflectivity factors the two models agree.

III. LINEAR STABILITY ANALYSIS

The existence of domain walls was already mentioned as being associated with the stability of the steady state solutions [5,6,9]. Since the linear stability analysis of the propagation model is only feasible with approximate solutions of the pump and signal amplitudes at the crystal exit [9], only the LSA of the mean-field solutions is presented here.

The homogeneous steady state ($\partial A_{0,1}/\partial\tau=\nabla^2 A_{0,1}=0$) of Eqs. (13) and (14) is given by (i) the nonlasing states $|\overline{A_0}|^2=E^2/(\gamma+\Delta_0^2)$ and $\overline{A_1^2}=0$, where the overbar refers to the homogeneous steady state, which is stable below the lasing threshold $E_{th}^2=(\gamma+\Delta_0^2)(1+\Delta_1^2)$; and (ii) the lasing states $\overline{A_0^2}=1+\Delta_1^2$ and $E^2=|\overline{A_1}|^4+2(\gamma-\Delta_0\Delta_1)|\overline{A_1}|^2+E_{th}^2$, called the HSS. Optical bistability occurs whenever the intensities of the signal field, $|\overline{A_1}|^2$, are multivalued function of the input intensity E^2, namely, if $\Delta_0\Delta_1>\gamma$ [12]. It was shown in Refs. [4,8,13,14] that homogeneous steady states of type (i) exhibit a pattern-forming instability at $E^2=E_M^2=(\gamma^2+\Delta_0^2)$, leading to periodical structures characterized by an intrinsic wavelength $\Lambda=2\pi/\sqrt{-\Delta_1}$. Thus, spontaneous pattern-forming instability requires $\Delta_1<0$ to have Λ real. In the following we shall focus on the linear stability analysis of a steady state of type (ii) with respect to Turing (modulational) and Hopf bifurcations. The LSA of the homogeneous steady state (ii), or HSS, with respect to a small perturbation of the form $\exp(\lambda t+i\mathbf{k}\cdot r)$, where $\mathbf{r}=(x,y)$ stands for the transverse coordinates and the wave vector $\mathbf{k}$ verifies the relation $(\nabla^2+k^2)\exp(\lambda t+i\mathbf{k}\cdot r)=0$, leads to the quartic characteristic equation

$$\lambda^4+2(\gamma+1)\lambda^3+f_1\lambda^2+f_2\lambda+f_3=0, \tag{15}$$

where

$$f_1=4|\overline{A_1}|^2+\delta_0^2+\delta_1^2+\gamma(4+\gamma)-\Delta_1^2, \tag{16}$$

$$f_2=4(\gamma+1)|\overline{A_1}|^2+2(\delta_0^2+\gamma\delta_1^2)+2\gamma(\gamma-\Delta_1^2), \tag{17}$$

$$f_3=4(\gamma+|\overline{A_1}|^2-\delta_0\delta_1)|\overline{A_1}|^2+(\gamma^2+\delta_0^2)(\delta_1^2-\Delta_1^2), \tag{18}$$

with $\delta_0=\Delta_0+\kappa^2/2$ and $\delta_1=\Delta_1+\kappa^2$. For the sake of simplicity, we consider the ratio between detuning parameters $\Delta_{0,1}$ equal to 2 or equivalently, $\delta_1=2\delta_0$.

For a given value of the pump input amplitude field E, Eq. (15) has four complex solutions $\lambda(\kappa^2)=\sigma(\kappa^2)\pm i\Omega(\kappa^2)$. The stability is derived from the largest growth rate $\sigma_m(\kappa^2)$, and the static or dynamical nature of the instability is given. For the numerical simulations considered in Sec. IV, with $\Delta_1=0$ and 1.5, the study of the largest growth rate shows that the homogeneous steady state is stable for a large domain of input intensity. For $\Delta_1=1.5$ the value of $\sigma(\kappa^2)$ is reported in Fig. 1 for two input amplitude $E=7$ and 20 above the threshold E_{th}.

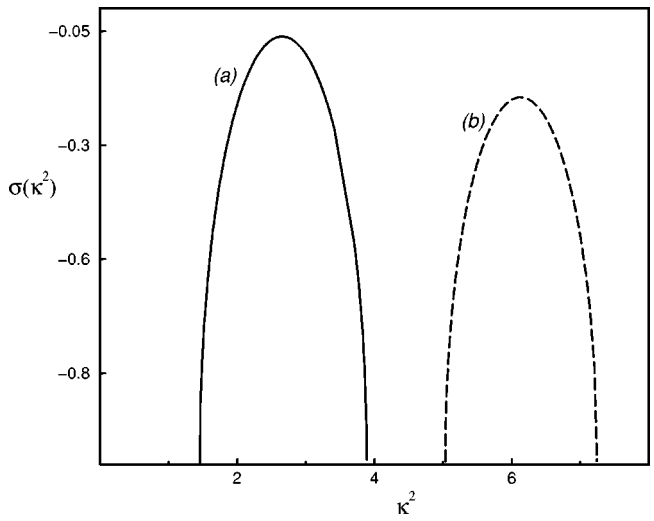

FIG. 1. Linear stability curves obtained for $\Delta_0=2\Delta_1=3$, and $\gamma=1$. We plot the growth rate of small-amplitude perturbations as a function of the square of the transverse wave number. (a) $E=7$. (b) $E=20$.

In the vicinity of the static threshold, an approximate value of the growth rate is $\sigma(\kappa^2)=-f_3/f_2$, as studied in Ref. [6]. At threshold, the conditions $f_3=0$ and $\partial f_3/\partial\kappa=0$ give

$$\kappa_M^2=-\Delta_1\pm\sqrt{\Delta_1^2/2-2\gamma^2+4|\overline{A}_{1M}|^2}, \tag{19}$$

where the critical intensity is given by

$$|\overline{A}_{1M}|^2=(\Delta_1^2+4\gamma^2)^2/16[4\gamma(\gamma+1)-\Delta_1^2]. \tag{20}$$

The latter relations show that the homogeneous steady state is stable for $\Delta_1<2$, in agreement with the exact solution of Eq. (15), and destabilizes through a modulational instability for $\Delta_1\geqslant 2$, as numerically observed in the propagation model [9].

For other values of detunings than those studied here, the homogeneous state can also exhibit a self-pulsing behavior (Hopf bifurcation [15]). The self-pulsing threshold intensity is given by $|\overline{A}_{1H}|^2=-\gamma(\gamma^2+\Delta_0^2)[\Delta_0^2+(\gamma+2)^2]/[2(\gamma+1)(\Delta_0^2+2\Delta_0\Delta_1+\gamma+\gamma^2)]$, and the pulsation frequency by $\Omega_H=2|\overline{A}_{1H}|^2+(\gamma^2+\Delta_0^2)/(1+\gamma)$. As we can see from the threshold expression, the self-pulsing instability requires $2\Delta_0\Delta_1<-(\gamma^2+\gamma+\Delta_0^2)$ to have $|\overline{A}_{1H}|^2$ real.

IV. STATIONARY AND TIME-PERIODIC BRIGHT SOLITONS

Two types of domain walls forming localized structures have been numerically observed. In the signal intensity pattern the structures appear as (i) a dark soliton in the form of a single stripe appearing spontaneously in the transverse plane [5,9], or (ii) a bright soliton with a circular domain

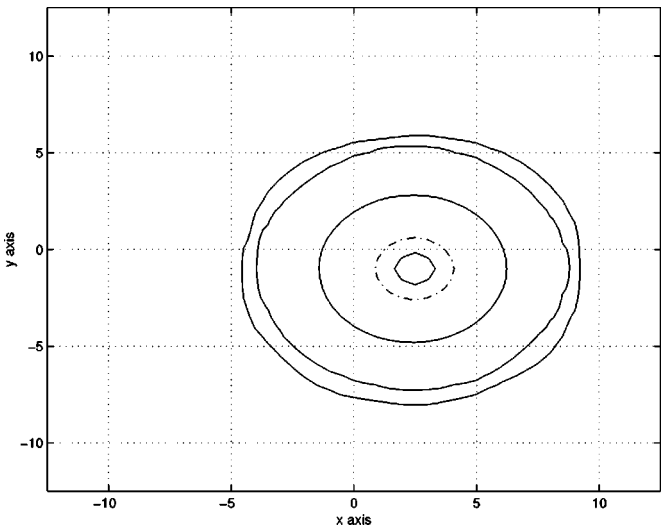

FIG. 2. The contour plot taken from Fig. 3. The solid (dotted) line represents the contours of the vanishing real (imaginary) part of the signal field. Parameters are $\Delta_0=3$, $\Delta_1=1.5$, $E=7$, and $\gamma=1$.

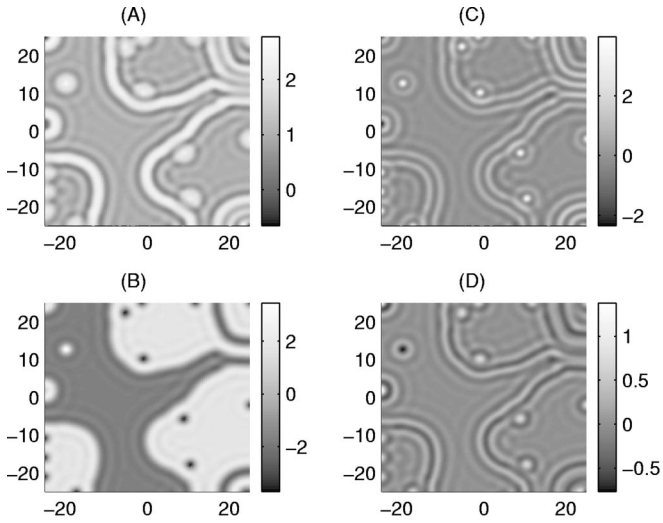

FIG. 3. Spontaneous formation of high-intensity localized structures. (a) and (b) Real parts of the pump and signal fields, respectively. (c) and (d) Imaginary parts of the pump and signal fields, respectively. Parameters are $\Delta_0=\Delta_1=0$, $\gamma=1$, and $E=4$. The initial condition consists of a small-amplitude random noise added to the homogeneous steady state (i). Maxima are plain white. Mesh number for the transverse integration 100×100.

wall [9,16]. The dark and bright solitons may coexist for the same value of the driving field [9], and their existences are not linked to a modulational instability. They are thus of a nature different from that of various LS's predicted in the bistable regime [17], and in the monostable regime where the HSS exhibits a subcritical modulational instability [18]. Actually both result from domain walls connecting two homogeneous lasing solutions of opposite sign, but they are not phase defects, since the real and imaginary parts of the signal amplitude never vanish at the same point. Consequently the signal phase undergoes a continuous variation along a line crossing the peak, and is defined everywhere in the transverse plane, as discussed in Ref. [9] for the propagation model, and as clearly visible in Fig. 2 for the mean-field model (cf. also Fig. 6 of Ref. [16], and Fig. 3 of Ref. [6]). The intensity is nowhere exactly equal to zero, but decreases close to zero in the region where the solution switches from a positive to a negative value; therefore, one infers that the situation is close to an Ising-Bloch transition.

We consider the two regimes where the homogeneous response curve exhibits a bistable behavior between the lasing and the nonlasing homogeneous steady states ($\Delta_0=2\Delta_1=3$) or a monostable behavior ($\Delta_0=\Delta_1=0$), with $\gamma=1$. For these parameters, the above LSA shows that the HSS's are stable with respect to both spatial and temporal instabilities (modulational and Hopf bifurcations). In these two regimes, stationary localized structures in the form of bright solitons with high-intensity peaks may be generated, showing that the existence of stable bright solitons is independent of bistability. They consist of one peak or more in the transverse plane. They are homoclinic solutions [19] (approaching the same HSS far from the peak), and their peak intensity in both transverse signal and pump profiles are much larger than those of the HSS. Here we consider only a numerical study of the bright solitons, an analytical approach to this problem being far beyond the scope of the present work.

We start our numerical simulations of the mean-field equations (13) and (14) by using the periodic boundary conditions in both transverse directions, and vary the injected signal E as the control parameter. In order to capture the bright solitons, we initially perturb the homogeneous unstable solutions by a small random noise. If this perturbation is randomly distributed in the transverse plane, the system evolves spontaneously toward the formation of randomly distributed bright and dark solitons (Fig. 3). The single bright soliton can also be generated for a positive detuning (see Fig. 4). An explicit Euler method, with finite differences for the diffraction operator, has been used. The time step $\Delta\tau$ has to be taken to be much smaller than the one required for the stability of the scheme in order that the numerical solution converges. Another study has been made using a semi-implicit Crank-Nicholson method both in time and transverse space [20]. The required $\Delta\tau$ to obtain the stationary solutions is ten times larger than the one of the Euler method. Then a good agreement between the stabilized values of the field intensities has been found with similar values of E. In fact, taking $\Delta\tau$ too large captures a temporal oscillatory profile of pump and signal fields whereas the same value of E gives stationary states for lower values of $\Delta\tau$.

With the propagation equations (1)–(4), a split and step method has been used with a 192×192 grid in the transverse plane and 20 steps for the axial propagation in the crystal. An explicit comparison between the results obtained from the mean-field equations (13) and (14) and the propagation model equations (1) and (4) is given in Figs. 5 and 6, where the maximum of the signal amplitude $|A_1|$ is reported as a function of the input pump amplitude E . The domain of the input amplitude for which stationary localized structures occur is generally smaller within the mean-field model than within the propagation model. In this domain, a good agree-

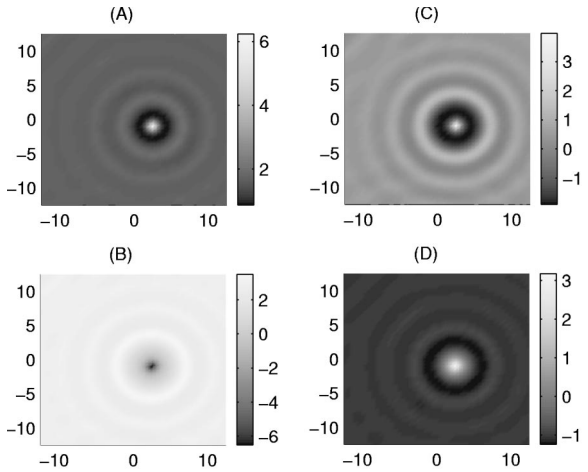

FIG. 4. Single high-intensity localized structures obtained by initially perturbing the homogeneous steady state (i) by a small-amplitude random noise. (a) and (b) Real parts of the pump and signal fields, respectively. (c) and (d) Imaginary parts of the pump and signal fields, respectively. Maxima are plain white. Parameters are $\Delta_0=3$, $\Delta_1=1.5$, $E=7$, and $\gamma=1$.

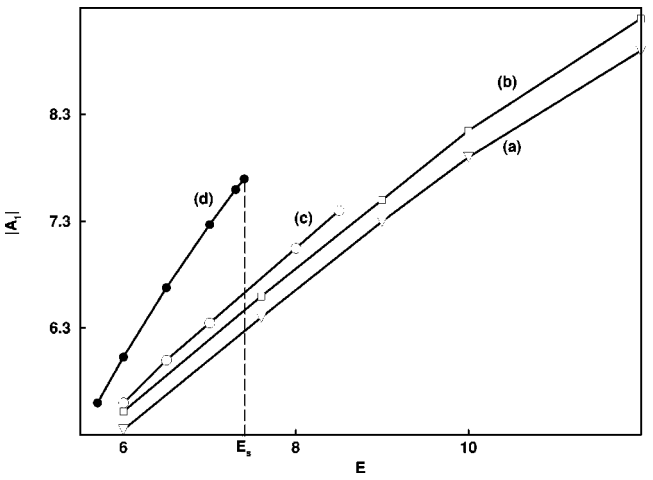

FIG. 6. Comparison between results obtained from the mean-field approximation, the propagation model, and the second-order corrections. We plot the amplitude of the localized structures as a function of the input field amplitude. Parameters are $\Delta_0=2\Delta_1=3$ and $\gamma=1$. [(a) and (b)], the propagation model for the reflectivity factors $R=0.9$ and 0.95, respectively. (c) The second-order Mac-Laurin expansion mapping model. (d) The mean-field model.

ment is displayed between both models. The agreement between the two models is much better for $\Delta_1=0$ (Fig. 5) than for $\Delta_1=1.5$ (Fig. 6). The peak intensities calculated within the propagation model very slightly vary with the transmittivity factor, so that the agreement between both models does not increase as the reflectivity factor R approaches unity, as shown in Fig. 6, where $R=R_{0,1}$ is varied from 0.9 to 0.95.

The second-order Mac-Laurin expansion mapping model was shown [9] to very well agree with the the full propagation model in a reduced domain of E. This agreement is illustrated in Fig. 6(c).

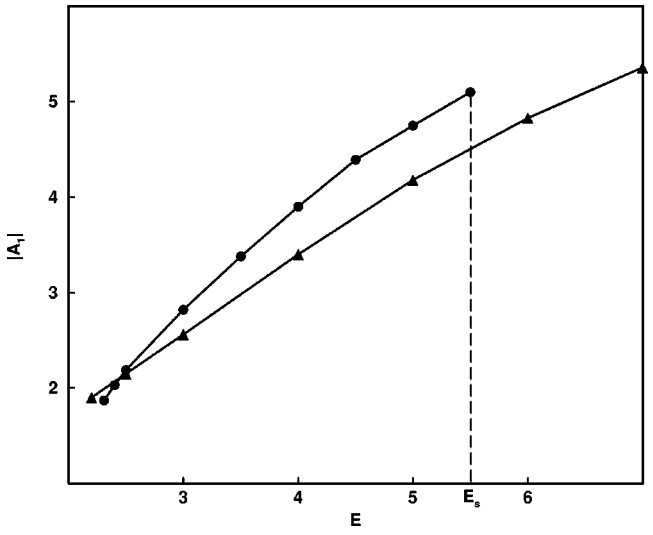

FIG. 5. Comparison beween results obtained at resonance $\Delta_0=\Delta_1=0$ and for $\gamma=1$. The circles indicate the high-amplitude localized structures obtained from the mean-field approximation. The triangles indicate the corresponding amplitude obtained from the propagation model.

We stress that the bright solitons are stationary only up to a certain value of the driving electric field $E=E_S$. For each detuning, the threshold E_S depends on the models.

As the driving field is increased, $E \geqslant E_S$, both signal and pump profiles start to oscillate regularly in time (see Fig. 7). This secondary instability appears only in the ''heart'' of the bright soliton, and does not affect the homogeneous background. The period of such a time oscillation is $T\approx 2.6$ for the mean-field model and $T\approx 1.8$ for the propagation model (with $R_1=0.9$), both in units of the cavity photon lifetime, and for $\Delta_1=0$. All mentioned results have been obtained in

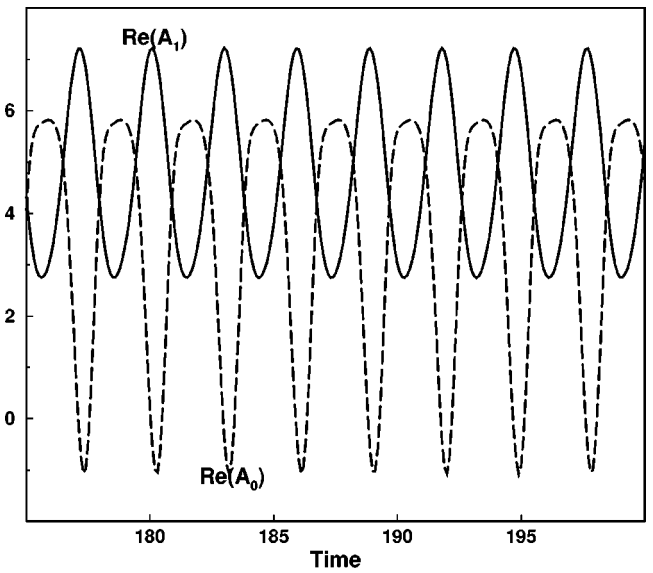

FIG. 7. Time evolution of the real part of the pump and signal fields. The parameters are $\Delta_0=\Delta_1=0$, $\gamma=1$, and $E=5.55$.

the regime where the HSS's are linearly stable with respect to the Hopf and modulational instabilities. These temporal oscillations, which are not due to the instability of the HSS's, arise as a secondary bifurcation from the soliton solutions, and are related to the intrinsic properties of the large intensity bright solitons.

V. CONCLUSION

The propagation equations describing the degenerated optical parametric oscillator completed with the cavity boundary conditions take the form of infinite-dimensional coupled maps. Following the procedure used in Ref. [8], this problem can be reduced, under the mean-field approximation, to two coupled partial differential equations. Detailed numerical studies of high-intensity localized structures in the two models indicate their existence in the monostable and bistable homogeneous regimes, in the parameter space where the homogeneous steady states are linearly stable. Let us point out that localized structures may also coexist with a weakly modulated steady state, i.e., very close to its modulational instability threshold [9].

The comparison between the two models reveals that the mean-field approximation is quite good as we approach the regime where both signal and pump fields are resonant with the optical cavity (zero cavity detuning). As the detunings increase, the agreement between the two models become less satisfying because the signal amplitude reaches value of order unit: First the intensity peak values differ, but above all because the existence domain of the stable bright solitons is strongly shortened in the mean-field model.

In both models, as the input fields increased, the high-intensity localized structures become unstable, and a time periodic regime appears. The temporal oscillations do not affect the homogeneous background, they are related to the stability properties of the high-intensity localized structure itself.

Let us emphasize that in the DOPO the smallest time is the response time τ_{rep} of the $\chi^{(2)}$ crystal, which is much smaller than the round trip time d. Consequently the condition used in Ref. [2] for the derivation of a mean-field equation, $d \ll \tau_{rep} \ll d/(1-R)$, is not fulfilled, for any value of the reflectivity. Nevertheless the above study proves that mean-field model for the DOPO is a qualitatively good, very useful to make analytical investigations, even for large intensity structures. We point out that second-order mapping model extends the range of pump parameter where analytical studies are still possible.

The comparative study of these three models will be pursued in the dynamical regime, where noticeable differences seem to appear. For example, in the case of DOPO with a saturable absorber, for a certain range of parameters where the mean-field model displays waves, a self-pulsing weak spatial chaos is observed with the propagation model [21].

ACKNOWLEDGMENTS

Stimulating discussions with Paul Mandel and René LeFever are gratefully acknowledged. This research was supported in part by the Inter-University Attraction Pole program of the Belgian government. The numerical simulations of the propagation equations were realized with the CRAY C90 of the IDRIS CNRS computer center, and their results were treated at the CRI of the Université Paris-Sud. The IDRIS center and the CRI are acknowledged for their services.

[1] L. A. Lugiato and R. Lefever, Phys. Rev. Lett. **58**, 2209 (1987).

[2] L. A. Lugiato, M. Brambilla, and A. Gatti, in *Advances in Atomic, Molecular and Optical Physics*, edited by B. Bedersen and H. Walther (Academic, New York, 1998).

[3] P. D. Drummond, K. J. Mc Neil, and D. F. Walls, Opt. Commun. **28**, 255 (1979); P. D. Drummond, K. J. Mc Neil, and D. F. Walls, Opt. Acta **27**, 321 (1980).

[4] G.L. Oppo, M. Brambilla, and L. A. Lugiato, Phys. Rev. A **49**, 2028 (1994).

[5] S. Trillo, M. Haelterman, and A. Sheppard, Opt. Lett. **22**, 970 (1997).

[6] K. Staliunas and V. J. Sanchez-Morcillo, Phys. Lett. A **241**, 28 (1998).

[7] V. B. Taranenko, K. Staliunas, and C. O. Weiss, Phys. Rev. Lett. **81**, 2236 (1998).

[8] M. Le Berre, D. Leduc, S. Patrascu, E. Ressayre, and A. Tallet, Chaos Solitons Fractals **10**, 627 (1999).

[9] M. Le Berre, D. Leduc, E. Ressayre, and A. Tallet, Quantum Semiclassic. Opt. **1**, 153 (1999).

[10] A. Yariv and P. Yeh, *Optical Waves in Crystals* (Wiley, New York, 1984).

[11] Originally the mean-field model was derived for a short delay as compared with the characteristic time of the material [1]. Here the response of the medium is instantaneous, so that the derivation for the OPO mean-field equations corresponds to the opposite limit.

[12] T. Debuisschert, A. Sizmann, E. Giacobino, and C. Fabre, J. Opt. Soc. Am. B **10**, 1668 (1993).

[13] M. Le Berre, E. Ressayre, and A. Tallet, Quantum Semiclassic. Opt. **1**, 107 (1999).

[14] K. Staliunas and V. J. Sanchez-Morcillo, Phys. Rev. A **57**, 1454 (1998).

[15] N. P. Pettiaux, R. D. Li, and P. Mandel, Opt. Commun. **72**, 256 (1989).

[16] G. L. Oppo, A. J. Scroggie, and W. J. Firth, Quantum Semiclassic. Opt. **1**, 133 (1999).

[17] N. N. Rosanov, G. Khodova, Opt. and Spektrosk. **65**, 449 (1988) [Opt. Spectrosc. **72**, 1394 (1992)]; a review of this group's activity is presented in N. N. Rosanov, Proc. SPIE **1840**, 130 (1992); also see the recent review paper by N. N. Rosanov, in *Progress in Optics* (North-Holland, Amesterdam, 1996) Vol. 35, pp. 1–60.

[18] M. Tlidi, P. Mandel, and R. Lefever, Phys. Rev. Lett. **73**, 640 (1994); M. Tlidi and P. Mandel, Chaos, Solitons and Fractals **4**, 1457 (1994).
[19] P. Coullet, C. Elphick, and D. Repaux, Phys. Rev. Lett. **58**, 431 (1987).
[20] L. Di Menza, Quantum Semiclassic. Opt. **1**, 19 (1999).
[21] M. Tlidi, L. Di Menza, M. Le Berre, E. Ressayre, and A. Tallet (unpublished).